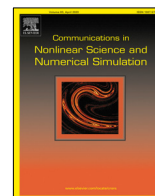




Contents lists available at ScienceDirect

# Communications in Nonlinear Science and Numerical Simulation

journal homepage: [www.elsevier.com/locate/cnsns](http://www.elsevier.com/locate/cnsns)

Research paper

## PINN deep learning method for the Chen–Lee–Liu equation: Rogue wave on the periodic background

Wei-Qi Peng<sup>a</sup>, Jun-Cai Pu<sup>a</sup>, Yong Chen<sup>a,b,\*</sup><sup>a</sup> School of Mathematical Sciences, Shanghai Key Laboratory of Pure Mathematics and Mathematical Practice, East China Normal University, Shanghai, 200241, China<sup>b</sup> College of Mathematics and Systems Science, Shandong University of Science and Technology, Qingdao, 266590, China

## ARTICLE INFO

## Article history:

Received 27 June 2021

Received in revised form 23 September 2021

Accepted 30 September 2021

Available online 7 October 2021

## Keywords:

The Chen–Lee–Liu equation

Rogue periodic wave

Breather wave

Soliton wave

Periodic wave

Physics-informed neural networks

Deep learning

## ABSTRACT

We consider the exact rogue periodic wave (rogue wave on the periodic background) and periodic wave solutions for the Chen–Lee–Liu equation via the odd-th order Darboux transformation. Then, the multi-layer physics-informed neural networks (PINNs) deep learning method is applied to research the data-driven rogue periodic wave, breather wave, soliton wave and periodic wave solutions of well-known Chen–Lee–Liu equation. Especially, the data-driven rogue periodic wave is learned for the first time to solve the partial differential equation. In addition, using image simulation, the relevant dynamical behaviors and error analysis for these solutions are presented. The numerical results indicate that the rogue periodic wave, breather wave, soliton wave and periodic wave solutions for Chen–Lee–Liu equation can be generated well by PINNs deep learning method.

© 2021 Elsevier B.V. All rights reserved.

## 1. Introduction

The derivative-type nonlinear Schrödinger equation can be considered as an appropriate model to describe some nonlinear phenomena in plasma astrophysics [1], fluid dynamics [2], and nonlinear optics [3,4]. The second type derivative nonlinear Schrödinger(DNLSII) equation is [5]

$$iq_t + q_{xx} + iq q^* q_x = 0, \quad (1)$$

where the asterisk \* means the complex conjugation. Eq. (1) is usually named Chen–Lee–Liu (CLL) equation, which was first introduced by Chen et al. [5]. The CLL equation is known as a model to simulate the propagation of the self-steepening optical pulses without self-phase modulation [6]. Using the Hirota method, the exact  $N$ -soliton solution of the CLL equation was constructed [7,8]. The breather solution, rogue wave solution and rational soliton solution have been obtained based on the Darboux transformation(DT) [9,10]. The initial–boundary value problem for the CLL equation was analyzed on the half line via the Fokas unified method [11]. There are other two types of derivative nonlinear Schrödinger equations, including first type derivative nonlinear Schrödinger(DNLSI) equation and third type derivative nonlinear Schrödinger(DNLSIII) equation. The DNLSI equation is [12]

$$q_t + iq_{xx} + (|q|^2 q)_x = 0. \quad (2)$$

\* Corresponding author at: School of Mathematical Sciences, Shanghai Key Laboratory of Pure Mathematics and Mathematical Practice, East China Normal University, Shanghai, 200241, China.

E-mail address: [ychen@sei.ecnu.edu.cn](mailto:ychen@sei.ecnu.edu.cn) (Y. Chen).

The DNLSIII takes the form [13]

$$iq_t + q_{xx} - iq^2q_x^* + \frac{1}{2}q^3(q^*)^2 = 0. \tag{3}$$

Through the gauge transformations, the three kinds of DNLS equations can be related to each other [14,15]. Eq. (2), also called the Kaup–Newell (KN) equation, can be used to describe the behaviors of small-amplitude Alfvén waves in a low- $\beta$  plasma [16–18] and large-amplitude magnetohydrodynamic (MHD) waves in a high- $\beta$  plasma [19,20]. In addition, the transmission of sub-picosecond pulses in single-mode fiber is described by Eq. (2) [21,22]. Eq. (3), known as Gerdjikov–Ivanov (GI) equation, was pioneered by Gerdjikov and Ivanov in Ref. [13]. Moreover, since the Eq. (3) has certain higher-order nonlinear effects, it can be viewed as an extension of the nonlinear Schrödinger(NLS) equation.

Rogue waves have been gradually reported in diverse fields, such as the deep ocean [23], the nonlinear optics [24] and Bose–Einstein condensation [25] and so on. Rogue waves appear out of nowhere and disappear into thin air, and the generation of rogue waves is related to the condition of baseband modulation instability (MI) [26]. Over the last few decades, rogue waves emerging on a plane wave background have been studied a lot and great progress has been made[27–33]. However, there are a great deal of work remains to be carried out for the rogue waves on the periodic background, which we call here as rogue periodic waves, and rogue periodic waves are more general and practical than ones on a plane wave background [34]. Therefore, more and more researchers have paid attention to rogue periodic waves for various integrable equations including the NLS equation, modified Korteweg–de Vries equation, Hirota equation, and sine–Gordon equation etc.[35–39]. However, to our knowledge, the rogue periodic waves for CLL equation (1) have not been studied. Thus, it is necessary and meaningful to study the rogue periodic waves for CLL equation. Without loss of generality, the construction of rogue periodic waves is usually associated with cumbersome Jacobian elliptic functions [35,40], but in this paper, we will apply a direct way to construct rogue periodic waves according to the odd-th order DT of the CLL equation.

Machine learning with the neural network method [41–43] has been widely applied in a variety of fields [44,45]. Especially, it plays a huge role in solving differential equations [46]. Recently, the physics-informed neural network (PINN) [47] and its improvement [48] have been proposed to solve many linear and nonlinear differential equations. In general, based on PINN deep learning method, accurate solutions can be obtained with very small amounts of data. At the same time, since the underlying physical constraints are usually explicitly depicted by differential equations, the method also gives a better physical explanation for the predicted solution. More recently, using PINN deep learning method, Chen group constructed data-driven soliton solutions for some nonlinear evolution equations [49–51] and data-driven high-order breather waves, rogue waves for the NLS equation and KN equation [52,53] with different initial and boundary conditions. Also, the data-driven rogue waves were studied for the defocusing NLS equation with a potential [54] and high-order NLS equation [55]. However, as far as we know, PINN deep learning for solving rogue periodic waves involving the partial differential equations has not been reported so far. Therefore, it will be very interesting and meaningful to research the data-driven rogue periodic wave via PINN deep learning method. Besides, the soliton wave, breather wave, periodic wave solutions of the CLL equation have not been investigated by the PINN deep learning method. For all of these reasons, we will aim at solving the data-driven rogue periodic wave, periodic wave, soliton wave and breather wave solutions for the CLL equation via deep learning.

The outline of this paper is organized as follows: In Section 2, the PINN deep learning method is introduced for the general (1+1)-dimensional nonlinear integrable systems. In Section 3, we derive the exact periodic wave solution and rogue periodic wave solution for the CLL equation (1) in terms of the odd-th order Darboux transformation (DT). In Section 4, by applying the PINN deep learning approach, the data-driven periodic wave, rogue periodic wave, soliton wave and breather wave solutions of the CLL equation (1) are investigated. In Section 5, we give some conclusions and discussions.

## 2. The PINN deep learning method

The (1+1)-dimensional complex nonlinear dispersive equations in its general form can be written as

$$q_t + \mathcal{N}_q(q, q_x, q_{xx}, q_{xxx}, \dots) = 0, \tag{4}$$

where  $q$  is a complex valued function with variables  $x$  and  $t$ . and  $\mathcal{N}_q$  is some nonlinear function of the  $q$  and its derivatives of arbitrary orders with respect to  $x$ . Taking  $q = u + iv$ , we decompose the above complex equation (4) into following two real nonlinear dispersive equations, given by

$$u_t + \mathcal{N}_u(u, u_x, u_{xx}, u_{xxx}, \dots) = 0, \tag{5}$$

$$v_t + \mathcal{N}_v(v, v_x, v_{xx}, v_{xxx}, \dots) = 0. \tag{6}$$

Then the physics-informed neural networks  $f_u(x, t)$  and  $f_v(x, t)$  can be defined as

$$f_u := u_t + \mathcal{N}_u(u, u_x, u_{xx}, u_{xxx}, \dots), \tag{7}$$

$$f_v := v_t + \mathcal{N}_v(v, v_x, v_{xx}, v_{xxx}, \dots), \tag{8}$$

where  $\mathcal{N}_u(u, u_x, u_{xx}, u_{xxx}, \dots)$ ,  $\mathcal{N}_v(v, v_x, v_{xx}, v_{xxx}, \dots)$  are the physical models given in Eq. (5), (6), and  $u(x, t; w, b)$ ,  $v(x, t; w, b)$  are the latent function of the deep neural network with the weight parameter  $w$  and bias parameter  $b$ , which can be used to approximate the exact complex-valued solution  $q(x, t)$  of objective equations. Then the networks  $f_u(x, t)$ ,  $f_v(x, t)$  can also be found with the help of automatic differentiation mechanism in deep learning [56]. By using the multi-hidden-layer deep neural network, the network parameters of the latent functions  $u, v$  and networks  $f_u(x, t)$  and  $f_v(x, t)$  can be constantly trained.

Throughout the training process, in order to obtain the optimum training results, we use L-BFGS optimization method [57] to minimize the whole mean squared error, that is, the loss function

$$Loss_{\Theta} = Loss_u + Loss_v + Loss_{f_u} + Loss_{f_v}, \tag{9}$$

where

$$Loss_u = \frac{1}{N_q} \sum_{i=1}^{N_q} |u(x_q^i, t_q^i) - u^i|^2, \quad Loss_v = \frac{1}{N_q} \sum_{i=1}^{N_q} |v(x_q^i, t_q^i) - v^i|^2, \tag{10}$$

and

$$Loss_{f_u} = \frac{1}{N_f} \sum_{j=1}^{N_f} |f_u(x_f^j, t_f^j)|^2, \quad Loss_{f_v} = \frac{1}{N_f} \sum_{j=1}^{N_f} |f_v(x_f^j, t_f^j)|^2, \tag{11}$$

where  $\{x_q^i, t_q^i, u^i\}_{i=1}^{N_q}$  and  $\{x_q^i, t_q^i, v^i\}_{i=1}^{N_q}$  are the sampled initial and boundary value training data of  $q(x, t)$ . Similarly, the collocation points for  $f_u(x, t)$  and  $f_v(x, t)$  are marked by  $\{x_f^j, t_f^j\}_{j=1}^{N_f}$  and  $\{x_f^j, t_f^j\}_{j=1}^{N_f}$ . The loss function (9) contains the losses of initial-boundary value data and the losses of networks (7) and (8) at a finite set of collocation points. Of which, the first two items on the right hand side of Eq. (9) attempt to let the learning solution approaches the exact one for the initial and boundary value data, and the latter two on the right hand side make the hidden  $u, v$  satisfy the target nonlinear dispersive equation (5), (6).

In this paper, the simple multilayer perceptrons (i.e., feedforward neural networks) with the Xavier initialization are chosen as the neural network model, and we select the hyperbolic tangent (tanh) as activation function. All codes are based on Python 3.7 and Tensorflow 1.15, and all numerical experiments shown here are run on a DELL Precision 7920 Tower computer with 2.10 GHz 8-core Xeon Silver 4110 processor and 64-GB memory.

### 3. The exact periodic wave and rogue periodic wave

In this section, we are committed to given the exact periodic wave and rogue periodic wave solutions for the CLL equation (1) via DT. The CLL equation (1) is associated with the following spectral problem

$$\begin{aligned} \Phi_x &= U\Phi = (-i\lambda^2 - \frac{i}{4}qr)\sigma_3\Phi + \lambda Q\Phi, \\ \Phi_t &= V\Phi = (-2i\lambda^4 - iqr\lambda^2 - \frac{1}{4}(qr_x - rq_x) - \frac{i}{8}q^2r^2)\sigma_3\Phi + 2\lambda^3Q\Phi + \lambda P\Phi, \end{aligned} \tag{12}$$

with

$$\begin{aligned} \Phi(x, t, \lambda) &= \begin{pmatrix} \phi(x, t, \lambda) \\ \varphi(x, t, \lambda) \end{pmatrix}, \quad \sigma_3 = \begin{pmatrix} 1 & 0 \\ 0 & -1 \end{pmatrix}, \quad Q = \begin{pmatrix} 0 & q \\ r & 0 \end{pmatrix}, \\ P &= \begin{pmatrix} 0 & iq_x + \frac{1}{2}q^2r \\ -ir_x + \frac{1}{2}r^2q & 0 \end{pmatrix}. \end{aligned} \tag{13}$$

Under the reduction condition  $r = -q^*$ , the CLL equation (1) can be raised by the compatibility condition (12). Moreover, to keep the above reduction condition invariant after each step DT, the Lax pair equations should meet following symmetry conditions as

- (1).  $\lambda_k = -\lambda_k^*$ ,  $\phi_k^*(x, t, \lambda_k) = \varphi_k(x, t, \lambda_k)$ ;
- (2).  $\lambda_{2k} = -\lambda_{2k-1}^*$ ,  $\phi_{2k-1}^*(x, t, \lambda_{2k-1}) = \varphi_{2k}(x, t, \lambda_{2k})$ ,  $\varphi_{2k-1}^*(x, t, \lambda_{2k-1}) = \phi_{2k}(x, t, \lambda_{2k})$ .

Let  $\Phi_k(x, t, \lambda_k) = [\phi_k(x, t, \lambda_k), \varphi_k(x, t, \lambda_k)]^T$  with  $T$  being the matrix transpose are the distinct solutions of Lax Pair (12) related to  $\lambda_k$ , and the seed solution is  $q^{[0]} = Ae^{i\theta}$ ,  $\theta = ax - (aA^2 + a^2)t$ , of which  $a$  and  $A$  being the complex parameters, then the  $N$ th order analytic solutions for CLL equation (1) are written into the following determinant expression [9,10]

$$q^{[N]} = e^{i\eta(\frac{1+(-1)^{N+1}}{2})} \left( \frac{q^{[0]} \det(S) + 2i \det(W)}{\det(S^*)} \right), \quad e^{i\eta} = e^{\frac{iA^2x}{2} - (iaA^2 + \frac{iA^4}{4})t}, \tag{14}$$

with  $W = (W_1, W_2, \dots, W_N)$ ,  $S = (S_1, S_2, \dots, S_N)$ , and

- (i)  $N = 2n + 1$ ,

$$W_k = (\varphi_k, \lambda_k\phi_k, \dots, \lambda_k^{2n-2}\varphi_k, \lambda_k^{2n-1}\phi_k, -\lambda_k^{2n+1}\phi_k)^T,$$

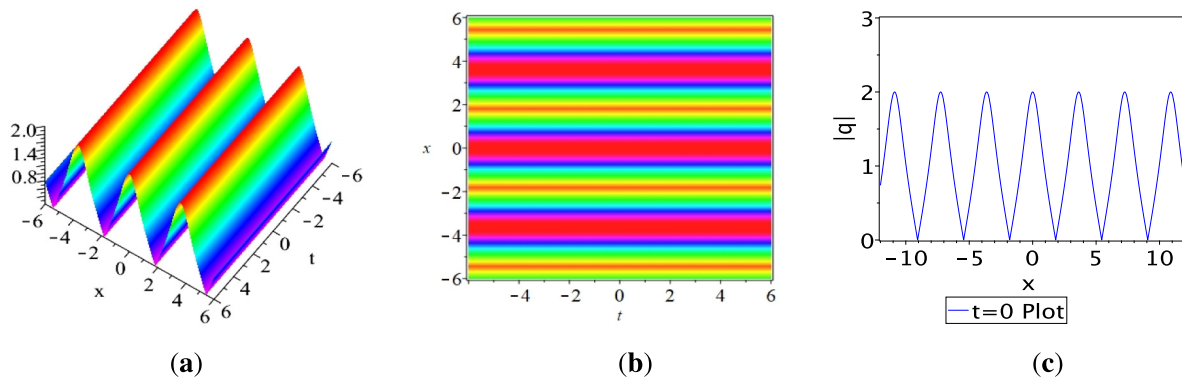


**Fig. 1.** The one periodic solution for Eq. (1) with parameter  $\beta = 0.5$ . (a) Three dimensional plot; (b) The density plot; (c) The wave propagation along the  $x$ -axis at  $t = 0$ .

$$S_k = (\varphi_k, \lambda_k \phi_k, \dots, \lambda_k^{2n-2} \varphi_k, \lambda_k^{2n-1} \phi_k, \lambda_k^{2n} \varphi_k)^T. \tag{15}$$

(ii)  $N = 2n$ ,

$$\begin{aligned} W_k &= (\phi_k, \lambda_k \varphi_k, \dots, \lambda_k^{2n-3} \varphi_k, \lambda_k^{2n-2} \phi_k, -\lambda_k^{2n} \phi_k)^T, \\ S_k &= (\phi_k, \lambda_k \varphi_k, \dots, \lambda_k^{2n-3} \varphi_k, \lambda_k^{2n-2} \phi_k, \lambda_k^{2n-1} \varphi_k)^T. \end{aligned} \tag{16}$$

Let  $q^{[0]} = Ae^{i\theta}$ ,  $\theta = ax - (aA^2 + a^2)t$  become the seed solution, and solving the Lax pair equation (12), we can obtain the corresponding vector eigenfunctions  $\Phi_k$  associated with  $\lambda_k$ , given by

$$\Phi_k(\lambda_k) = \begin{pmatrix} \phi_k(x, t, \lambda_k) \\ \varphi_k(x, t, \lambda_k) \end{pmatrix} = \begin{pmatrix} \psi_1(\lambda_k) + \psi_2^*(-\lambda_k^*) \\ \psi_2(\lambda_k) + \psi_1^*(-\lambda_k^*) \end{pmatrix}, \tag{17}$$

with

$$\begin{pmatrix} \psi_1(\lambda_k) \\ \psi_2(\lambda_k) \end{pmatrix} = \begin{pmatrix} \frac{-i(A^2 - 4\lambda_k^2 - 2a + s)}{4\lambda_k} e^{\frac{i}{2}(s/2)x + bt + \theta} \\ Ae^{\frac{i}{2}(s/2)x + bt - \theta} \end{pmatrix}, \tag{18}$$

where

$$\begin{aligned} s &= \sqrt{A^4 + 8\lambda_k^2 A^2 + 16\lambda_k^4 - 4A^2 a + 16a\lambda_k^2 + 4a^2}, \\ b &= \frac{A^2}{4} - 2A^2 \lambda_k^2 + 4\lambda_k^4 - \frac{A^2}{4}(A^2 - 4\lambda_k^2 - 2a + s) \\ &\quad + \lambda_k^2(A^2 - 4\lambda_k^2 - 2a + s) - \frac{a}{2}(A^2 - 4\lambda_k^2 - 2a + s) - a^2. \end{aligned} \tag{19}$$

For CLL equation (1), as presented in Ref. [9,10], the rational solution, breather wave and rogue wave on the constant background have been constructed via expression (14) when  $N = 2n$ . However, we hereby try to construct the periodic wave and rogue periodic wave for CLL equation by taking  $N = 2n + 1$  in expression (14).

Taking  $N = 1$ , and  $A = 1, a = -1$  in Eq. (14), the exact one periodic wave solution is derived as

$$q(x, t) = e^{\frac{i}{2}x + \frac{3i}{4}t} \left( \frac{q^{[0]}\varphi_1(\lambda_1) - 2i\lambda_1\phi_1(\lambda_1)}{\varphi_1^*(\lambda_1)} \right) = \frac{M_1}{N_1} \tag{20}$$

with

$$\begin{aligned} M_1 &= (8\beta^3 + 2c\beta + 2\beta)e^{-\frac{1}{8}ic(4t\beta^2 - t - 2x) + \frac{3it}{4}} + (-4\beta^2 + c + 3)e^{\frac{1}{8}ic(4t\beta^2 - t - 2x) + \frac{3it}{4}}, \\ N_1 &= (3 + 4\beta^2 + c)e^{-\frac{1}{8}ic(4t\beta^2 - t - 2x) - \frac{it}{2}} - 4\beta e^{\frac{1}{8}ic(4t\beta^2 - t - 2x) - \frac{it}{2}}, \end{aligned} \tag{21}$$

where  $c = \sqrt{16\beta^4 + 8\beta^2 + 9}$ , and  $\beta$  is the arbitrary constant. The dynamic behaviors of exact one periodic wave solution are shown in Fig. 1, and it is obvious that the solution (20) is a periodic solution in the  $x$  direction.

Let  $N = 2n + 1, \lambda_1 = \frac{\sqrt{-2a}}{2} + \frac{i}{2}A, \lambda_2 = -\lambda_1^*$  and  $\lambda_N = i\beta$ . By taking Taylor expansion as [58,59] in (14) for  $N = 2n + 1$ , the exact  $n$ th rogue periodic wave solution can be given by

$$q^{[n]} = e^{in} \left( \frac{q^{[0]}\det(\tilde{S}) + 2i\det(\tilde{W})}{\det(\tilde{S}^*)} \right), \tag{22}$$

with

$$\tilde{W} = \begin{pmatrix} \varphi[1, 0, 1] & \varphi[2, 0, 1] & \varphi[1, 0, 2] & \varphi[2, 0, 2] & \cdots & \varphi[1, 0, n] & \varphi[2, 0, n] & \varphi_N \\ \phi[1, 1, 1] & \phi[2, 1, 1] & \phi[1, 1, 2] & \phi[2, 1, 2] & \cdots & \phi[1, 1, n] & \phi[2, 1, n] & \lambda_N \phi_N \\ \vdots & \vdots & \vdots & \vdots & \cdots & \vdots & \vdots & \vdots \\ \varphi[1, N-3, 1] & \varphi[2, N-3, 1] & \varphi[1, N-3, 2] & \varphi[2, N-3, 2] & \cdots & \varphi[1, N-3, n] & \varphi[2, N-3, n] & \lambda_N^{N-3} \varphi_N \\ \phi[1, N-2, 1] & \phi[2, N-2, 1] & \phi[1, N-2, 2] & \phi[2, N-2, 2] & \cdots & \phi[1, N-2, n] & \phi[2, N-2, n] & \lambda_N^{N-2} \phi_N \\ -\phi[1, N, 1] & -\phi[2, N, 1] & -\phi[1, N, 2] & -\phi[2, N, 2] & \cdots & -\phi[1, N, n] & -\phi[2, N, n] & -\lambda_N^N \phi_N \end{pmatrix}, \tag{23}$$

$$\tilde{S} = \begin{pmatrix} \varphi[1, 0, 1] & \varphi[2, 0, 1] & \varphi[1, 0, 2] & \varphi[2, 0, 2] & \cdots & \varphi[1, 0, n] & \varphi[2, 0, n] & \varphi_N \\ \phi[1, 1, 1] & \phi[2, 1, 1] & \phi[1, 1, 2] & \phi[2, 1, 2] & \cdots & \phi[1, 1, n] & \phi[2, 1, n] & \lambda_N \phi_N \\ \vdots & \vdots & \vdots & \vdots & \cdots & \vdots & \vdots & \vdots \\ \varphi[1, N-3, 1] & \varphi[2, N-3, 1] & \varphi[1, N-3, 2] & \varphi[2, N-3, 2] & \cdots & \varphi[1, N-3, n] & \varphi[2, N-3, n] & \lambda_N^{N-3} \varphi_N \\ \phi[1, N-2, 1] & \phi[2, N-2, 1] & \phi[1, N-2, 2] & \phi[2, N-2, 2] & \cdots & \phi[1, N-2, n] & \phi[2, N-2, n] & \lambda_N^{N-2} \phi_N \\ \varphi[1, N-1, 1] & \varphi[2, N-1, 1] & \varphi[1, N-1, 2] & \varphi[2, N-1, 2] & \cdots & \varphi[1, N-1, n] & \varphi[2, N-1, n] & \lambda_N^{N-1} \varphi_N \end{pmatrix}, \tag{24}$$

where

$$\phi[l, j, n] = \frac{1}{n!} \frac{\partial^{2n}}{\partial \epsilon^{2n}} [(\lambda_l + \epsilon^2)^j \phi(\lambda_l + \epsilon^2)], \quad \varphi[l, j, n] = \frac{1}{n!} \frac{\partial^{2n}}{\partial \epsilon^{2n}} [(\lambda_l + \epsilon^2)^j \varphi(\lambda_l + \epsilon^2)]. \tag{25}$$

Taking  $N = 3$  and  $A = 1, a = -1$  in Eq. (22) and using Maple symbolic computation, the exact one rogue periodic wave solution can be given by

$$q(x, t) = \frac{M_3}{D_3}, \tag{26}$$

with

$$\begin{aligned} M_3 &= -96\beta M_3^+ e^{-\frac{1}{8}ic(4t\beta^2-t-2x)+\frac{3it}{4}} - 48M_3^- e^{\frac{1}{8}ic(4t\beta^2-t-2x)+\frac{3it}{4}}, \\ D_3 &= D_3^+ e^{-\frac{1}{8}ic(4t\beta^2-t-2x)-\frac{ix}{2}} + 96\beta D_3^- e^{\frac{1}{8}ic(4t\beta^2-t-2x)-\frac{ix}{2}}, \\ M_3^+ &= c[(\frac{x^2}{4} + (\frac{t}{2} + \frac{i}{6})x + \frac{1}{12} + \frac{3t^2}{4})\beta^2 + \frac{x^2}{16} + (\frac{t}{8} + \frac{7i}{24})x - \frac{1}{6} + \frac{3t^2}{16} + \frac{it}{4}] \\ &+ (x^2 + (2t + \frac{2i}{3})x + \frac{1}{3} + 3t^2)\beta^4 + (\frac{x^2}{2} + (t + \frac{4i}{3})x - \frac{1}{6} + \frac{3t^2}{2} + it)\beta^2 \\ &+ \frac{9x^2}{16} + (\frac{5i}{8} + \frac{9t}{8})x + \frac{27t^2}{16} - \frac{3it}{4} - \frac{9}{16}, \\ M_3^- &= c[(\frac{x^2}{4} + (\frac{t}{2} + \frac{i}{6})x + \frac{1}{12} + \frac{3t^2}{4})\beta^2 - \frac{3x^2}{16} + (-\frac{3t}{8} + \frac{i}{8})x + \frac{3}{16} - \frac{9t^2}{16} + \frac{3it}{4}] \\ &- (x^2 + (2t + \frac{2i}{3})x + \frac{1}{3} + 3t^2)\beta^4 + (-\frac{x^2}{2} - (t + \frac{4i}{3})x + \frac{3}{2} - \frac{3t^2}{2} + it)\beta^2 \\ &- \frac{9x^2}{16} + (\frac{3i}{8} - \frac{9t}{8})x - \frac{27t^2}{16} + \frac{9it}{4} + \frac{9}{16}, \\ D_3^+ &= c[(-12x^2 + (8i - 24t)x - 36t^2 - 4)\beta^2 - 9x^2 - (6i + 18t)x - 27t^2 - 3] \\ &+ (-48x^2 + (32i - 96t)x - 144t^2 - 16)\beta^4 + (-24x^2 + (-32i - 48t)x \\ &- 96it - 72t^2 - 40)\beta^2 - 27x^2 - (18i + 54t)x - 81t^2 - 9, \\ D_3^- &= c[-\frac{x^2}{8} + (\frac{i}{12} - \frac{t}{4})x + \frac{it}{4} + \frac{1}{24} - \frac{3t^2}{8}] + (it + \frac{1}{3})\beta^2 + \frac{3it}{4} + \frac{ix}{2} + \frac{1}{4}. \end{aligned} \tag{27}$$

The dynamic behaviors of exact one rogue periodic wave solution (26) are shown in Fig. 2. From Fig. 2, it is easily to find that there is a rogue wave that arises in a background of periodic wave, and the rogue wave is distributed in the region where the periodic wave reaches its amplitude.

In general, it is not hard to see that the higher-order rogue periodic wave solution can be generated by Eq. (22). However, due to their complex expressions showing these solutions, we just give some plots (see Fig. 3) of the two-order rogue periodic wave solution by taking  $N = 5$  in Eq. (22). In what follows, we would like to use the PINN deep learning scheme to investigate the data-driven periodic wave, one rogue periodic wave, soliton wave and breather wave of the CLL equation (1).

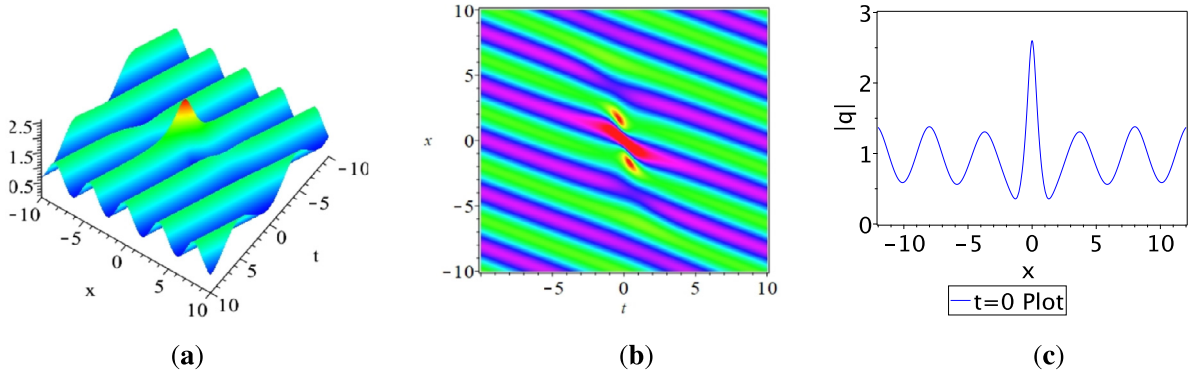


**Fig. 2.** The one rogue periodic wave solution (26) for Eq. (1) with parameter  $\beta = -0.2$ . (a) Three dimensional plot; (b) The density plot; (c) The wave propagation along the  $x$ -axis at  $t = 0$ .

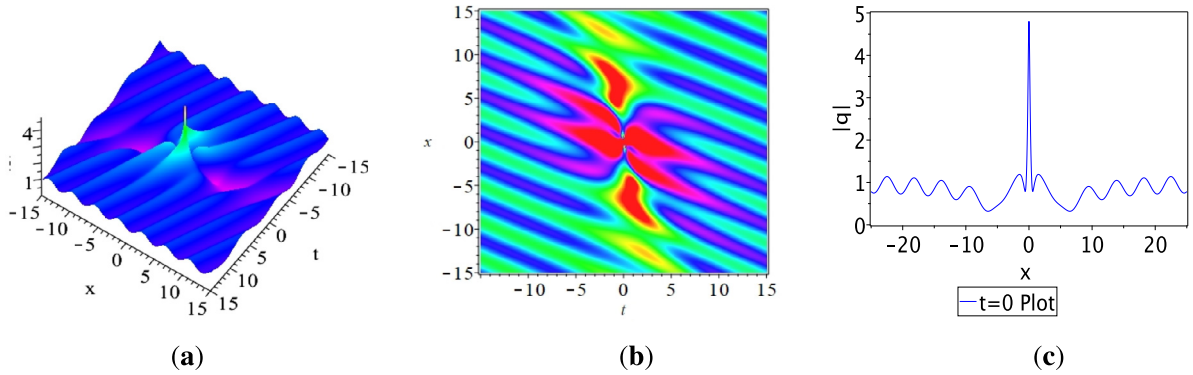


**Fig. 3.** The two rogue periodic wave solution for Eq. (1) with parameter  $\beta = -0.1$  and  $A = 1, a = -1$ . (a) Three dimensional plot; (b) The density plot; (c) The wave propagation along the  $x$ -axis at  $t = 0$ .

#### 4. The data-driven periodic wave, rogue periodic wave, soliton wave, and breather wave

In the beginning, we focus on the CLL equation (1) along with Dirichlet boundary conditions

$$\begin{cases} iq_t + q_{xx} + iq q^* q_x = 0, & x \in [x_0, x_1], t \in [t_0, t_1], \\ q(x, t_0) = q_0(x), \\ q(x_0, t) = q_1(t), \quad q(x_1, t) = q_2(t), \end{cases} \quad (29)$$

where  $x_0, x_1$  denote the corresponding boundaries of  $x$ .  $t_0, t_1$  are initial and final times of  $t$ . The  $q_0(x)$  defines the initial condition. The physics-informed neural networks  $f_u(x, t)$  and  $f_v(x, t)$  for the above equation (29) can be defined as

$$\begin{aligned} f_u &:= -v_t + u_{xx} - (u^2 + v^2)v_x, \\ f_v &:= u_t + v_{xx} + (u^2 + v^2)u_x, \end{aligned} \quad (30)$$

In terms of the PINN scheme, we can define respectively the complex valued neural network  $q(x, t) = u(x, t) + iv(x, t)$  and  $f(x, t) = f_u + if_v$  into follows by Python:

```
def net_q(self, x, t):
    q = self.neural_net(tf.concat([x, t], 1), self.weights, self.biases)
    u = q[:, 0 : 1]
    v = q[:, 1 : 2]
    return u, v
def net_f(self, x, t):
    u, v = self.net_q(x, t)
    u_t = tf.gradients(u, t)[0]
    u_x = tf.gradients(u, x)[0]
    u_xx = tf.gradients(u_x, x)[0]
    v_t = tf.gradients(v, t)[0]
```

```

v_x = tf.gradients(v, x)[0]
v_xx = tf.gradients(v_x, x)[0]
f_u = -v_t + u_xx - (u**2 + v**2) * v_x
f_v = u_t + v_xx + (u**2 + v**2) * u_x
return f_u, f_v
    
```

Next, we will apply the PINN deep learning approach to solve the data-driven periodic wave, rogue periodic wave, soliton wave, and breather wave solutions for the CLL equation (1) in detail.

#### 4.1. The data-driven periodic wave solution

Taking  $\beta = 0.5$  into Eq. (20) and let  $[x_0, x_1]$  and  $[t_0, t_1]$  in Eq. (29) as  $[-6.0, 6.0]$  and  $[0.0, 2.0]$ , respectively. We here select the periodic wave solution at  $t = 0$  as the initial condition, given by

$$q(x, 0) = q_0(x) = \frac{2(\sqrt{3} + 1) \cos(\frac{\sqrt{3}}{2}x)}{(2 + \sqrt{3})e^{\frac{(\sqrt{3}-1)ix}{2}} - e^{-\frac{(\sqrt{3}+1)ix}{2}}}. \tag{31}$$

To acquire the original training data, the traditional finite difference method is used to simulate Eq. (29) with the initial data (31) by MATLAB. Of which, the spatial region  $[-6.0, 6.0]$  is divided into 513 points and time region  $[0, 2.0]$  is divided into 401 points. Then, via using the Latin hypercube sampling (LHS) method [60], we randomly extract  $N_q = 100$  from the original initial boundary data and  $N_f = 10\,000$  collocation points to generate a small training dataset containing a subset of the initial boundary. According to obtained training data, using a 9-hidden-layer deep PINN with 40 neurons per layer, the periodic wave solution  $q(x, t)$  is successfully learned by regulating the network parameters and minimize the loss function (9). The  $\mathbb{L}_2$ -norm error between learning solution and exact solution is  $1.141566e-02$ . The whole learning process takes about 1530.5031 s, and iterates 13070 times.

Fig. 4(a), (b), (c), (d) display the wave propagation plot at three different times, the density plot, the three-dimensional motion, the error density diagram, and the loss curve figure, respectively. From Fig. 4(a) and (b), we can find that the error between the learning solution and the exact solution is very small. As shown in Fig. 4(d), the loss curve is quite smooth. These results demonstrate the integrable deep learning method is effective and stable.

#### 4.2. The data-driven rogue periodic wave solution

In this part, we devote to research the data-driven rogue periodic wave solution for CLL equation (1). Taking  $\beta = -0.02$  into Eq. (26) and let  $[x_0, x_1]$  and  $[t_0, t_1]$  in Eq. (29) as  $[-12.0, 12.0]$  and  $[-1.5, 1.5]$ , respectively. We select the rogue periodic wave solution at  $t = -1.5$  as the initial condition

$$q(x, -1.5) = q_0(x) = \frac{-11250K_1^+ e^{\frac{3\sqrt{97691}i}{1562500}(1250x-936)-\frac{9i}{8}} + K_1^- e^{-\frac{3\sqrt{97691}i}{1562500}(1250x-936)-\frac{9i}{8}}}{K_2^+ e^{\frac{\sqrt{97691}i}{781250}(1875x-1404)-\frac{ix}{2}} + 11250K_2^- e^{-\frac{\sqrt{97691}i}{781250}(1875x-1404)-\frac{ix}{2}}}, \tag{32}$$

with

$$\begin{aligned}
 K_1^+ &= \sqrt{97691} \left( \frac{313x^2}{1250} + \left( \frac{2188i}{1875} - \frac{939}{1250} \right) x + \frac{4321}{3000} - \frac{3i}{2} \right) \\
 &+ \frac{293073x^2}{1250} + \left( \frac{488698i}{1875} - \frac{879219}{1250} \right) x + \frac{12133723}{9000} + \frac{937i}{2}, \\
 K_1^- &= \sqrt{97691} (-210825x^2 + (632475 + 140700i)x + \frac{4848375}{4} - 1265625i) \\
 &- 65941425x^2 + (197824275 + 43882800i)x - \frac{1516465375}{4} - 395578125i, \\
 K_2^+ &= \sqrt{97691} (211050x^2 + (140550i - 633150)x + \frac{2989875}{2}) \\
 &+ 65941425x^2 + (43976550i - 197824275)x + \frac{1868465375}{4} - 140625i, \\
 K_2^- &= \sqrt{97691} \left( -\frac{x^2}{2} + \left( \frac{3}{2} + \frac{i}{3} \right) x - \frac{77}{24} - \frac{3i}{2} \right) + \frac{938}{9} - 469i + \frac{625ix}{3}.
 \end{aligned} \tag{33}$$

$$\begin{aligned}
 K_2^- &= \sqrt{97691} \left( -\frac{x^2}{2} + \left( \frac{3}{2} + \frac{i}{3} \right) x - \frac{77}{24} - \frac{3i}{2} \right) + \frac{938}{9} - 469i + \frac{625ix}{3}.
 \end{aligned} \tag{34}$$

Here, applying the same data discretization method in Section 4.1, we generate the initial and boundary value dataset with the spatial region  $[-12.0, 12.0]$  dividing into 513 points and temporal region  $[-1.5, 1.5]$  into 401 points. With the help of LHS, a training dataset can be obtained by random sampling  $N_q = 400$  in the original dataset and choosing  $N_f = 10\,000$  collocation points. Inputting the training dataset into a 9-hidden-layer deep PINN with the first layer is 40 neurons, and the rest is 60 neurons, we successfully generate the learning rogue periodic wave solution which has a  $\mathbb{L}_2$  error of  $6.103918e-03$  compared with the exact one. The whole learning process takes about 3551.8307 s, and the

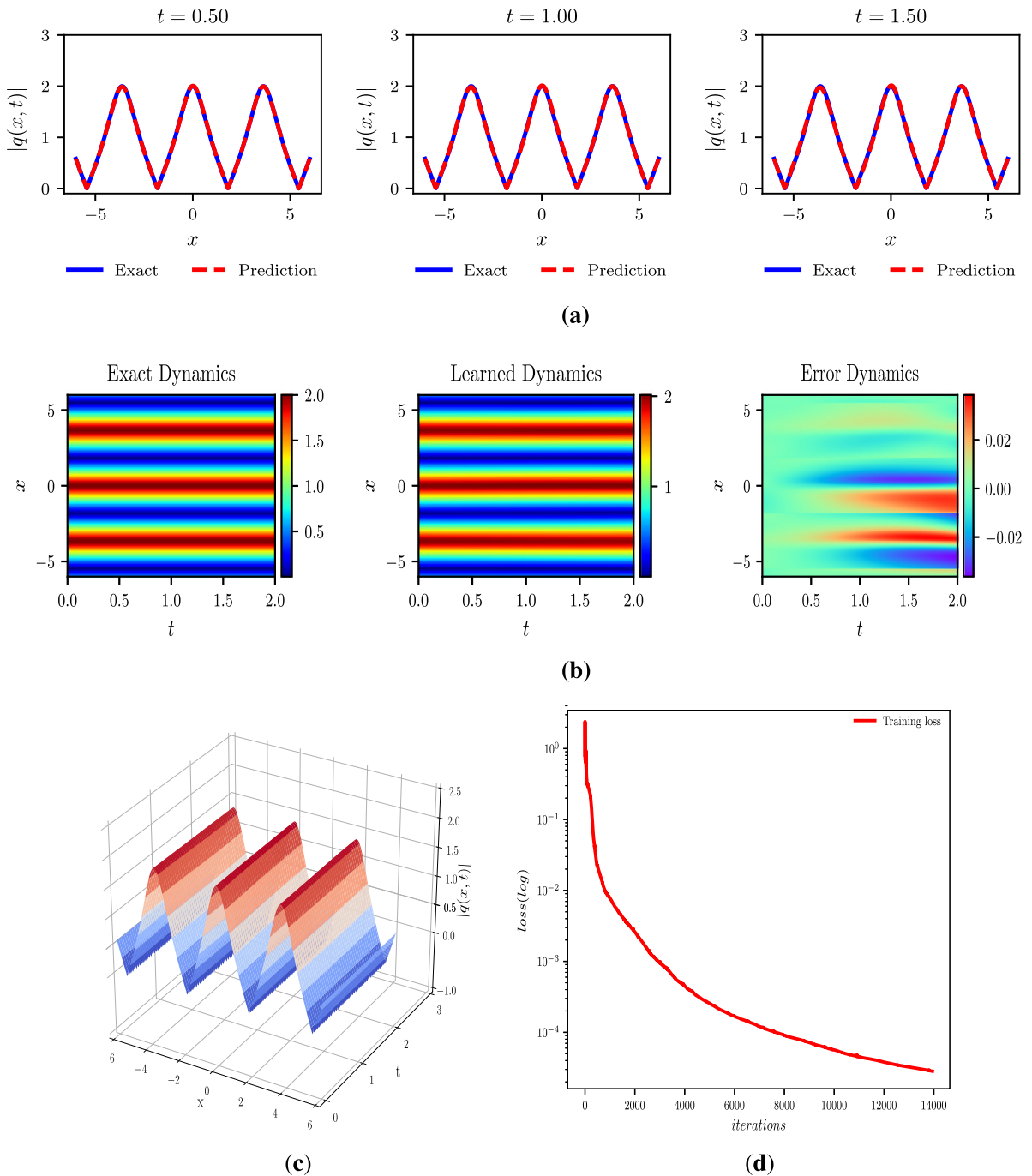


**Fig. 4.** The data-driven periodic wave solution  $q(x, t)$  for CLL equation (29): (a) The wave propagation plot at three different times; (b) The density plot and the error density diagram; (c) The three-dimensional plot; (d) The loss curve figure.

iteration times is 28208. Due to the rogue periodic wave solution is more multifarious compared with the periodic wave solution, we here choose the bigger sample points and more neurons. However, this does not mean that more neurons are better. When we take 60 neurons per layer, the experiment results are even worse with a  $\mathbb{L}_2$  error of  $1.560081e-02$ , training time of 3915.8433 and 31053 number of iterations.

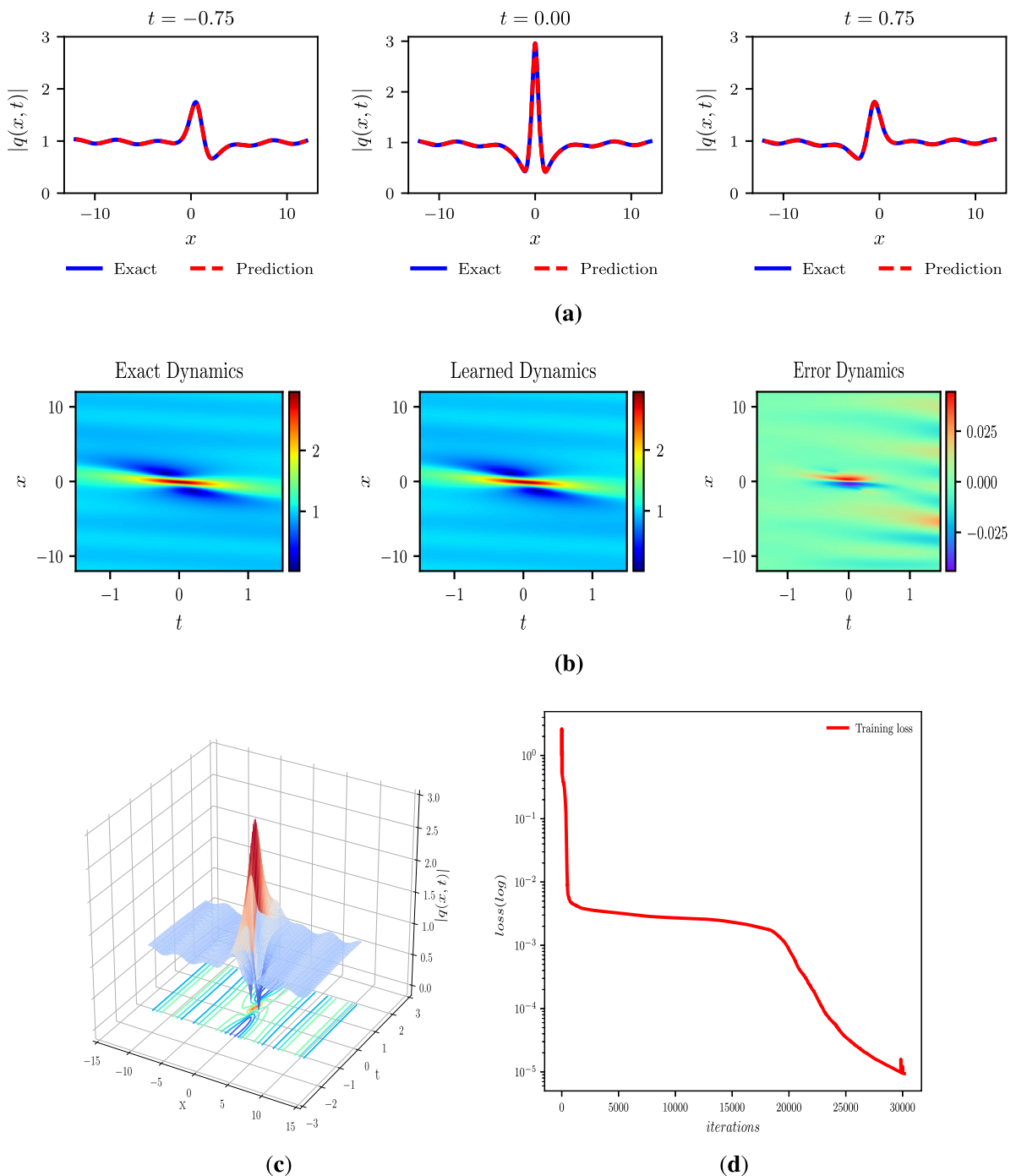


**Fig. 5.** The data-driven rogue periodic wave solution  $q(x, t)$  for CLL equation (29): (a) The wave propagation plot at three different times; (b) The density plot and the error density diagram; (c) The three-dimensional plot; (d) The loss curve figure.

The main results of our experiment are displayed in Fig. 5 including the wave propagation plot at different time, the density plots for the learning rogue periodic wave solution and exact rogue periodic wave solution, error dynamics diagrams, three dimensional plot and loss curve plot. Through Fig. 5(a) and (b), we present a comparison between the exact solution and the learning solution, and it is not hard to find the error is very small. Interestingly, from Fig. 5(d), we can observe that the loss curve is like “stair”, which does not exist in that one of periodic wave solution.

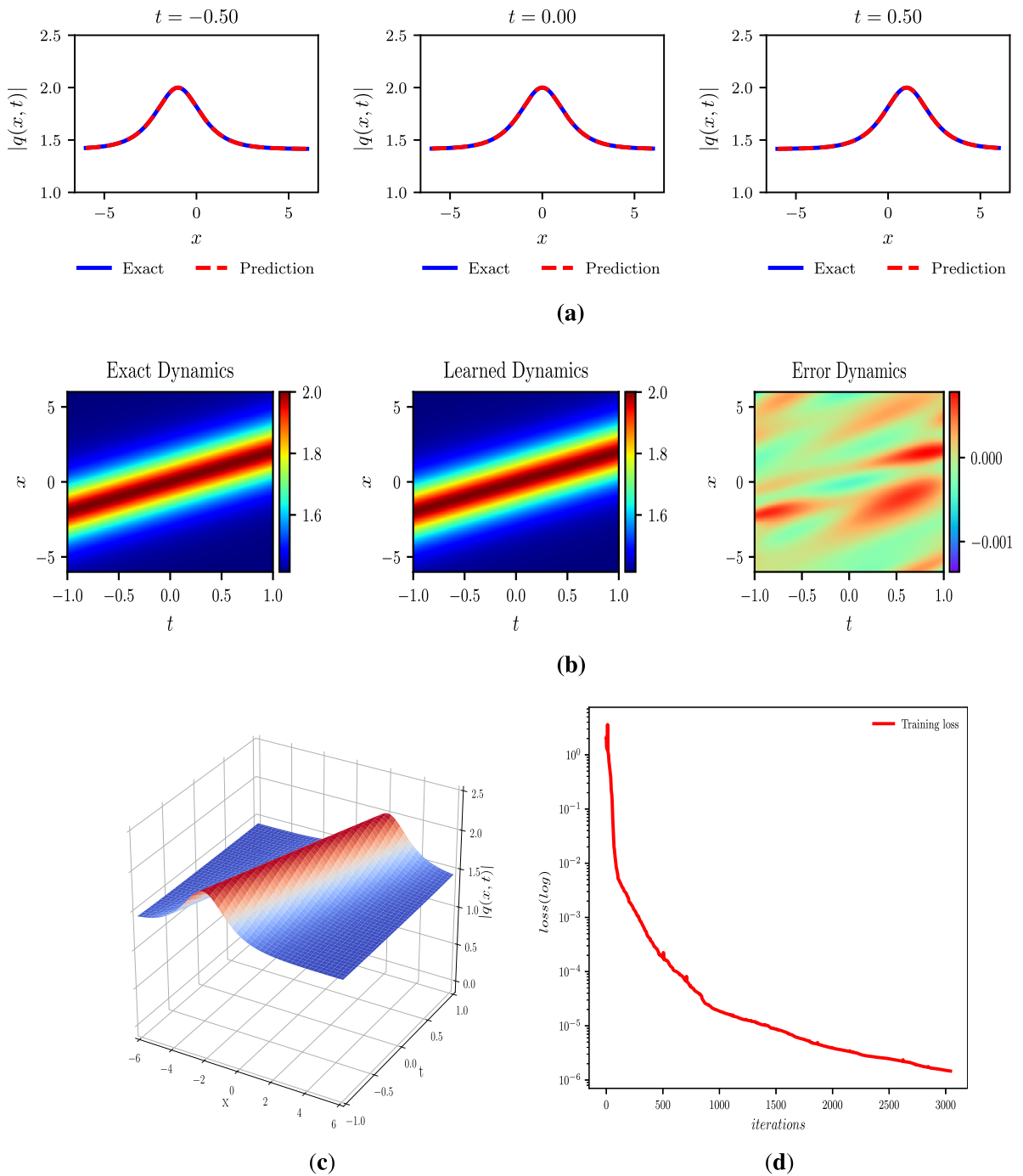


**Fig. 6.** The data-driven bright soliton wave solution  $q(x, t)$  for CLL equation (29): **(a)** The wave propagation plot at three different times; **(b)** the density plot and the error density diagram; **(c)** The three-dimensional plot; **(d)** The loss curve figure.

### 4.3. The data-driven soliton wave solution

As shown in Ref. [10], the expression (59) of Ref. [10] will be the bright soliton solution with taking  $a = c = 1, \beta = 0.5$ , and be the dark soliton solution with taking  $a = c = 1, \beta = -0.5$ . Let  $[x_0, x_1]$  and  $[t_0, t_1]$  in Eq. (29) as  $[-6.0, 6.0]$  and  $[-1.0, 1.0]$  respectively, the corresponding initial condition for the bright soliton solution is given by

$$q(x, -1) = q_0(x) = \frac{(1 + i)(e^{2 + \frac{5i}{4} + (1 + \frac{i}{2})x} + e^{\frac{i}{4}(2x+5)})}{ie^{x+2} + 1}. \tag{35}$$

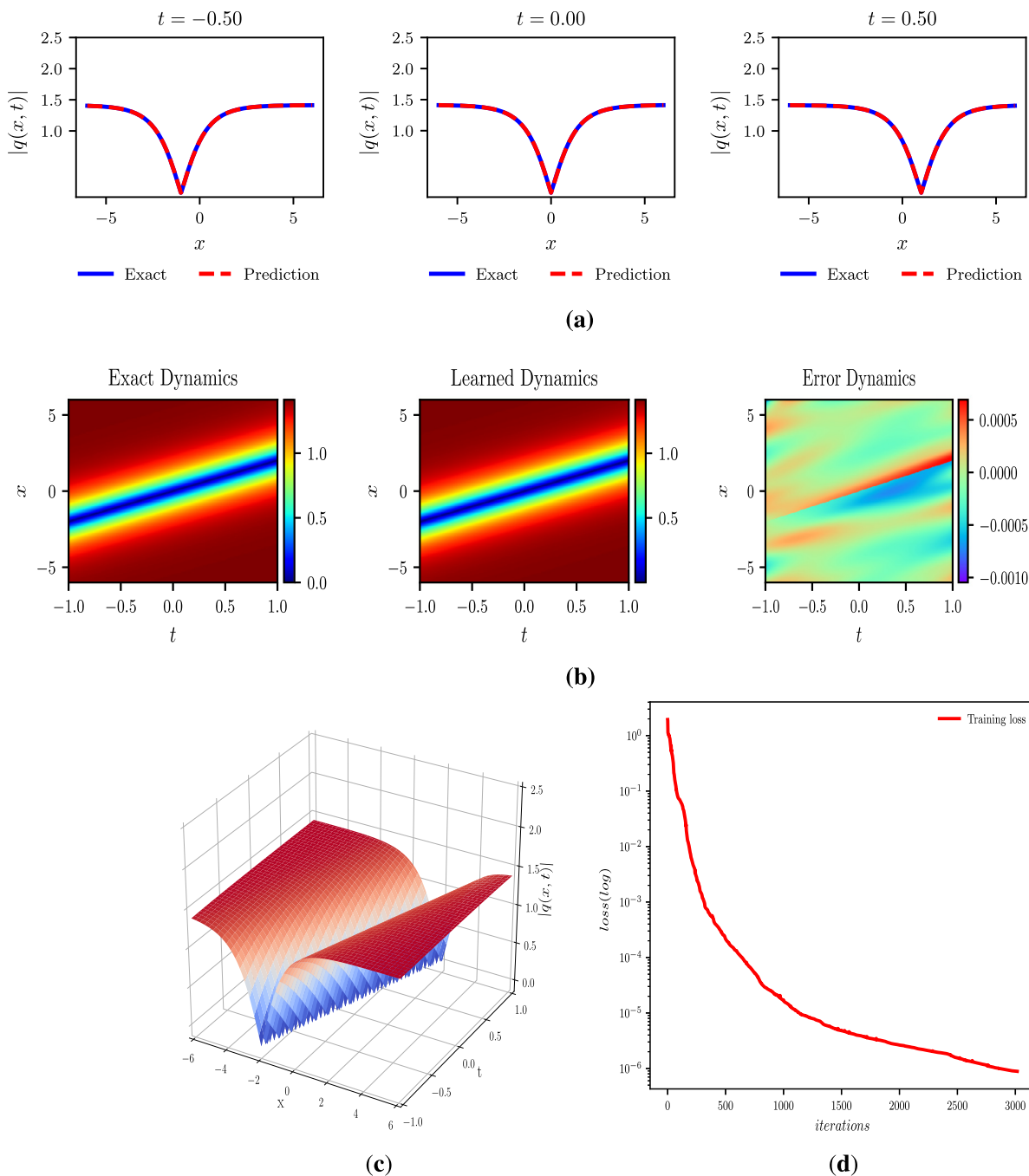


**Fig. 7.** The data-driven dark soliton wave solution  $q(x, t)$  for CLL equation (29): (a) The wave propagation plot at three different times; (b) The density plot and the error density diagram; (c) The three-dimensional plot; (d) The loss curve figure.

For the dark soliton solution, the initial condition becomes

$$q(x, -1) = q_0(x) = \frac{-(1 + i)(e^{2 + \frac{5i}{4} + (1 + \frac{i}{2})x} + (1 + i)e^{\frac{i}{4}(2x+5)})}{ie^{x+2} - 1}. \tag{36}$$

Via performing the same data acquisition and training procedures as Section 4.1, it is found, for bright soliton solution, the  $\mathbb{L}_2$ -norm error between learning solution and exact solution is  $1.410725e-04$ , the whole learning process takes about 352.3080 s, and iterates 3153 times. For dark soliton solution, the  $\mathbb{L}_2$ -norm error between learning solution and

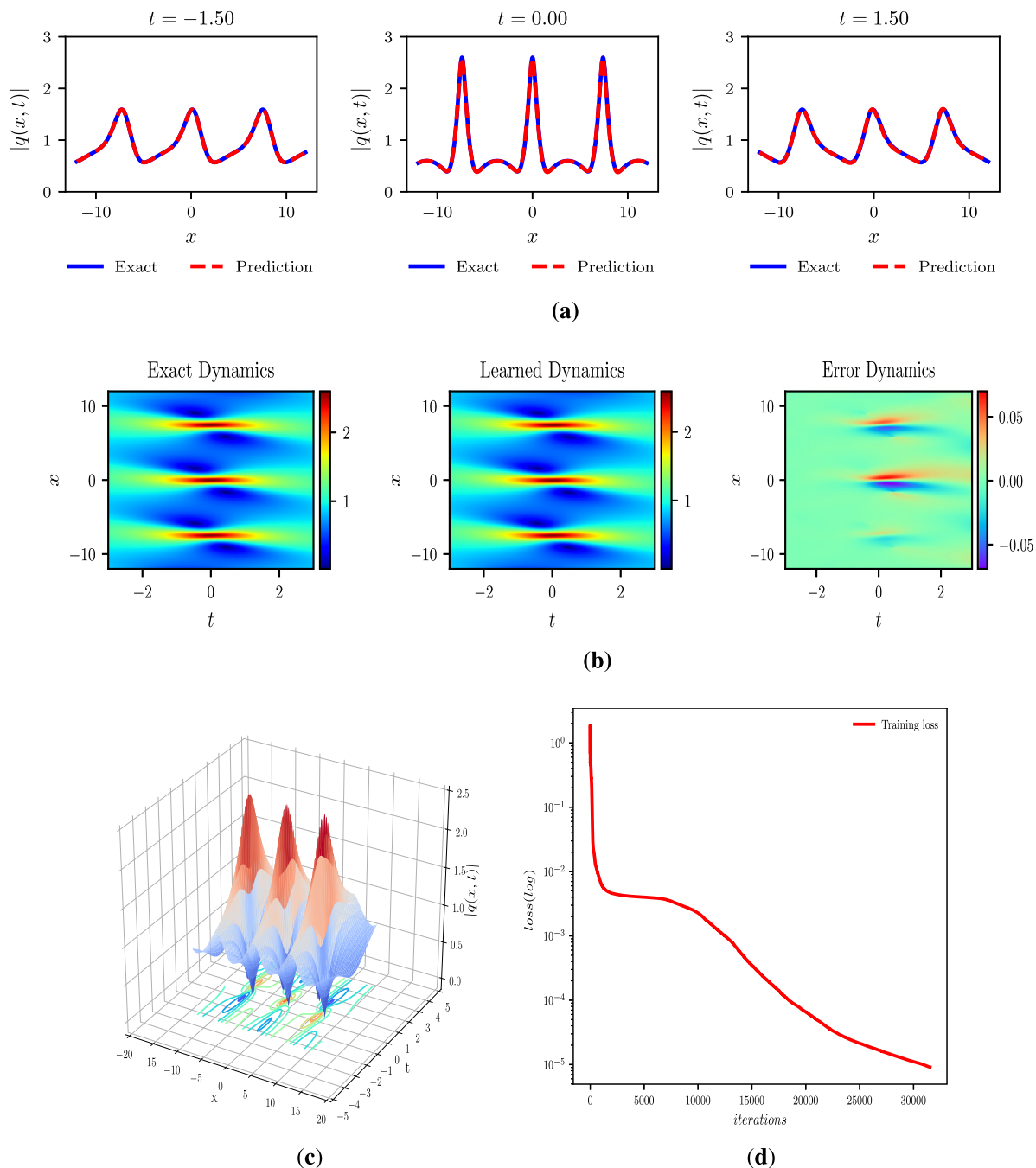


**Fig. 8.** The data-driven breather wave solution  $q(x, t)$  for CLL equation (29): (a) The wave propagation plot at three different times; (b) The density plot and the error density diagram; (c) The three-dimensional plot; (d) The loss curve figure.

exact solution is  $3.660262e-04$ , the whole learning process takes about 225.7577 s, and iterates 2147 times. Fig. 6 and Fig. 7 display the relevant learning outcomes for the bright soliton and dark soliton, respectively. According to these experimental results, we find the learning effect for soliton is quite good.

#### 4.4. The data-driven breather wave solution

Taking  $c = 1, \alpha_1 = 0.5, \beta_1 = 0.4$ , into expression (60) in Ref. [10], and let  $[x_0, x_1]$  and  $[t_0, t_1]$  in Eq. (29) as  $[-12.0, 12.0]$  and  $[-3.0, 3.0]$ , respectively, and we here select  $t = -3$  as the initial condition for the breather wave solution, given

by

$$q(x, -1) = q_0(x) = \frac{60i(\sqrt{2} - \frac{3}{5}) \sin(\frac{3\sqrt{2}(25x-27)}{125}) e^{-\frac{17i}{625}(25x+24)} - H_1 e^{-\frac{17i}{625}(25x+24)}}{H_2}, \quad (37)$$

where

$$\begin{aligned} H_1 &= 180\sqrt{2}i \sinh(\frac{36\sqrt{2}}{25}) - 108i \sinh(\frac{36\sqrt{2}}{25}) - 21\sqrt{2} \cosh(\frac{36\sqrt{2}}{25}) \\ &+ 60\sqrt{2} \cos(\frac{3\sqrt{2}(25x-27)}{125}) - 200 \cos(\frac{3\sqrt{2}(25x-27)}{125}) + 70 \cosh(\frac{36\sqrt{2}}{25}), \\ H_2 &= (60\sqrt{2} - 200) \cos(\frac{3\sqrt{2}(25x-27)}{125}) + (60\sqrt{2}i - 36i) \sin(\frac{3\sqrt{2}(25x-27)}{125}) \\ &+ (250 - 75\sqrt{2}) \cosh(\frac{36\sqrt{2}}{25}) + 60(\sqrt{2} - \frac{3}{5})i \sinh(\frac{36\sqrt{2}}{25}). \end{aligned} \quad (38)$$

Using the same data discretization method as in Section 4.1, we obtain the initial and boundary value dataset with the spatial region  $[-12.0, 12.0]$  dividing into 513 points and temporal region  $[-3.0, 3.0]$  into 401 points. Being different from the case of Section 4.1, we take the  $N_q = 400$  boundary sample point and  $N_f = 20\,000$  collocation points. Besides, a 9-hidden-layer deep PINN with 60 neurons per layer is chosen here. After training, the neural network model reaches a  $\mathbb{L}_2$  error of  $1.156422e-02$  compared with the exact one. The whole learning process takes about 4212.7363 s, and the iteration times is 29376. Fig. 8 presents the relevant dynamical behaviors and error analysis for the breather wave solution. Being analogous to the loss curve of rogue periodic wave solution, there is a gentle interregion for the loss curve in Fig. 8(d).

## 5. Conclusion

In this paper, we have applied the odd-th order DT to derive the exact periodic wave and rogue periodic wave for CLL equation (1). Then, in terms of the obtained exact solutions, PINN deep learning method was introduced to solve the periodic wave and rogue periodic wave involving the CLL equation (1). It is worth mentioning that the deep learning for the rogue periodic wave is first realized to solve the partial differential equation. Furthermore, we applied the PINN deep learning approach to solve the data-driven soliton wave and breather wave solutions for CLL equation (1). Our results indicate that the errors between the exact solutions with the ones generated by PINN deep learning method is very small, which verifies the integrable deep learning method is effective and stable. Compared with the traditional numerical methods, the PINN deep learning method has no grid size limitation. In addition, due to physical constraints, the network is trained with only a small amount of data and has better physical interpretation. This method opens up a new way to solve the integrable and unintegrable systems by using deep learning and find some novel models in the interdisciplinary field of applied mathematics and computational science. Remarkably, by selecting a certain time domain, PINN method has a good training effect. However, with a wider range of time interval, the training effect will not be as good as we expected. Especially for rogue periodic wave, the effect is only good in a small time range. Therefore, in the future, we will solve the problem about how to simulate the rogue periodic wave well in a large spatio-temporal scale, such as using a reservoir computing approach, or selecting the corresponding Lax pairs equation as the physical constraints rather than the equation itself.

## CRedit authorship contribution statement

**Wei-Qi Peng:** Writing – original draft, Writing – review & editing, Conceptualization, Formal analysis, Software. **Jun-Cai Pu:** Writing – review & editing, Supervision. **Yong Chen:** Writing – review & editing, Supervision, Project administration.

## Declaration of competing interest

The authors declare that they have no known competing financial interests or personal relationships that could have appeared to influence the work reported in this paper.

## Acknowledgments

The project is supported by National Natural Science Foundation of China (No. 12175069), Global Change Research Program of China (No. 2015CB953904) and Science and Technology Commission of Shanghai Municipality (No. 18dz2271000).

## References

- [1] Rogister A. Parallel propagation of nonlinear low-frequency waves in high- $\beta$  plasma. *Phys Fluids* 1971;14(12):2733–9.
- [2] Johnson RS. On the modulation of water waves in the neighbourhood of  $kh \approx 1.363$ . *Proc R Soc Lond Ser A Math Phys Eng Sci* 1977;357(1689):131–41.
- [3] Anderson D, Lisak M. Nonlinear asymmetric self-phase modulation and self-steepening of pulses in long optical waveguides. *Phys. Rev. A* 1983;27(3):1393.
- [4] Kodama Y. Optical solitons in a monomode fiber. *J Stat Phys* 1985;39(5):597–614.
- [5] Chen HH, Lee YC, Liu CS. Integrability of nonlinear Hamiltonian systems by inverse scattering method. *Phys Scr* 1979;20:490–2.
- [6] Moses J, Malomed BA, Wise FW. Self-steepening of ultrashort optical pulses without self-phase-modulation. *Phys. Rev. A* 2007;76:021802.
- [7] Nakamura A, Chen HH. Multi-soliton solutions of a derivative nonlinear Schrödinger equation. *J Phys Soc Japan* 1980;49:813–6.
- [8] Kakei S, Sasa N, Satsuma J. Bilinearization of a generalized derivative nonlinear Schrödinger equation. *J Phys Soc Japan* 1995;64:1519–23.
- [9] Yang B, Zhang WG, Zhang HQ, et al. Generalized darboux transformation and rational soliton solutions for Chen–Lee–Liu equation. *Appl Math Comput* 2014;242:863–76.
- [10] Zhang YS, et al. Darboux transformation of the second-type derivative nonlinear Schrödinger equation. *Lett. Math. Phys.* 2015;105(6):853–91.
- [11] Zhang N, Xia TC, Fan EG. A Riemann–Hilbert approach to the Chen–Lee–Liu equation on the half line. *Acta Math. Appl. Sin-E* 2018;34(3):493–515.
- [12] Kaup DJ, Newell AC. An exact solution for a derivative nonlinear Schrödinger equation. *J Math Phys* 1978;19:798–801.
- [13] Gerdjikov VS, Ivanov I. A quadratic pencil of general type and nonlinear evolution equations. II. Hierarchies of Hamiltonian structures. *Bulg. J. Phys.* 1983;10:130–43.
- [14] Kakei S, Sasa N, Satsuma J. Bilinearization of a generalized derivative nonlinear Schrödinger equation. *J Phys Soc Japan* 1995;64:1519–23.
- [15] Kundu A. Exact solutions to higher-order nonlinear equations through gauge transformation. *Physica D* 1987;25:399–406.
- [16] Mio K, Ogino T, Minami K, et al. Modified nonlinear Schrödinger equation for Alfvén waves propagating along the magnetic field in cold plasmas. *J Phys Soc Japan* 1976;41(1):265–71.
- [17] Mjølhus E. Nonlinear Alfvén waves and the DNLS equation: oblique aspects. *Phys. Scr.* 1989;40(2):227.
- [18] Mjølhus E. On the modulational instability of hydromagnetic waves parallel to the magnetic field. *J. Plasma Phys.* 1976;16(3):321–34.
- [19] Fedun V, Ruderman MS, Erdélyi R. Generation of short-lived large-amplitude magnetohydrodynamic pulses by dispersive focusing. *Phys. Lett. A* 2008;372(39):6107–10.
- [20] Ruderman MS. DNLS equation for large-amplitude solitons propagating in an arbitrary direction in a high- $\beta$  hall plasma. *J. Plasma Phys.* 2002;67(4):271–6.
- [21] Anderson D, Lisak M. Nonlinear asymmetric self-phase modulation and self-steepening of pulses in long optical waveguides. *Phys. Rev. A* 1983;27(3):1393–8.
- [22] Tzoar N, Jain M. Self-phase modulation in long-geometry optical waveguides. *Phys. Rev. A* 1981;23(3):1266.
- [23] Pelinovsky E, Kharif C. *Extreme ocean waves*. Berlin: Springer; 2008.
- [24] Solli DR, Ropers C, Jalali B. Active control of rogue waves for stimulated supercontinuum generation. *Phys Rev Lett* 2008;101(23):233902.
- [25] Bludov YV, Konotop VV, Akhmediev N. Matter rogue waves. *Phys. Rev. A* 2009;80(3):033610.
- [26] Zhang GQ, Yan ZY, Wen XY. Modulational instability, beak-shaped rogue waves, multi-dark-dark solitons and dynamics in pair-transition-coupled nonlinear Schrödinger equations. *Proc R Soc Lond Ser A Math Phys Eng Sci* 2017;473(2203):20170243.
- [27] Li RM, Geng XG. A matrix yajima-oikawa long-wave-short-wave resonance equation, Darboux transformations and rogue wave solutions. *Commun Nonlinear Sci Numer Simul* 2020;90:105408.
- [28] Guo BL, Ling LM, Liu QP. Nonlinear Schrödinger equation: generalized darboux transformation and rogue wave solutions. *Phys Rev E* 2012;85:026607.
- [29] Wang X, Li YQ, Chen Y. Generalized Darboux transformation and localized waves in coupled Hirota equations. *Wave Motion* 2014;51(7):1149–60.
- [30] He JS, Tao YS, Porsezian K, Fokas AS. Rogue wave management in an inhomogeneous nonlinear fibre with higher order effects. *J Nonlinear Math Phys* 2013;20(3):407–19.
- [31] Chen SH, Song LY. Rogue waves in coupled Hirota systems. *Phys Rev E* 2013;87:032910.
- [32] Zhang GQ, Yan ZY, Wen XY, Chen Y. Interactions of localized wave structures and dynamics in the defocusing coupled nonlinear Schrödinger equations. *Phys Rev E* 2017;95:042201.
- [33] Sun WR, Wang L. Matter rogue waves for the three component Gross–Pitaevskii equations in the spinor Bose–Einstein condensates. *Proc R Soc Lond Ser A Math Phys Eng Sci* 2018;474:20170276.
- [34] Kedziora DJ, Ankiewicz A, Akhmediev N. Rogue waves and solitons on a cnoidal background. *Eur. Phys. J-Spec. Top.* 2014;223(1):43–62.
- [35] Chen JB, Pelinovsky DE. Rogue periodic waves of the modified KdV equation. *Nonlinearity* 2018;31(5):1955.
- [36] Chen JB, Pelinovsky DE. Rogue periodic waves of the focusing nonlinear Schrödinger equation. *Proc R Soc Lond Ser A Math Phys Eng Sci* 2018;474(2210):20170814.
- [37] Peng WQ, Tian SF, Wang XB, et al. Characteristics of rogue waves on a periodic background for the Hirota equation. *Wave Motion* 2020;93:102454.
- [38] Gao X, Zhang HQ. Rogue waves for the Hirota equation on the Jacobi elliptic  $cn$ -function background. *Nonlinear Dynam.* 2020;101(2):1159–68.
- [39] Li RM, Geng XG. Rogue periodic waves of the sine-Gordon equation. *Appl Math Lett* 2020;102:106147.
- [40] Kedziora DJ, Ankiewicz A, Akhmediev N. Rogue waves and solitons on a cnoidal background. *Eur. Phys. J-Spec. Top.* 2014;223(1):43–62.
- [41] McCulloch WS, Pitts W. A logical calculus of the ideas immanent in nervous activity. *Bull. Math. Biophys.* 1943;5:115–33.
- [42] Rosenblatt F. The perceptron: A probabilistic model for information storage and organization in the brain. *Psychol. Rev.* 1958;65(6):386–408.
- [43] Bryson AE, Ho YC. *Applied optimal control: Optimization, estimation, and control*. Taylor and Francis; 1975.
- [44] LeCun Y, Bengio Y, Hinton G. Deep learning. *Nature* 2015;521(7553):436–44.
- [45] Goodfellow I, Bengio Y, Courville A. *Deep learning*. MIT Press; 2016.
- [46] Lagaris IE, Likas A, Fotiadis DI. Artificial neural networks for solving ordinary and partial differential equations. *IEEE Trans Neural Netw* 1998;9(5):987–1000.
- [47] Raissi M, Perdikaris P, Karniadakis GE. Physics-informed neural networks: A deep learning framework for solving forward and inverse problems involving nonlinear partial differential equations. *J Comput Phys* 2019;378:686–707.
- [48] Jagtap AD, Kharazmi E, Karniadakis GE. Conservative physics-informed neural networks on discrete domains for conservation laws: Applications to forward and inverse problems. *Comput Methods Appl Mech Engrg* 2020;365:113028.
- [49] Li J, Chen Y. Solving second-order nonlinear evolution partial differential equations using deep learning. *Commun Theor Phys* 2020;72:105005.
- [50] Li J, Chen Y. A deep learning method for solving third-order nonlinear evolution equations. *Commun Theor Phys* 2020;72:115003.
- [51] Li J, Chen Y. A physics-constrained deep residual network for solving the sine-Gordon equation. *Commun Theor Phys* 2020;73(1):015001.
- [52] Pu JC, Li J, Chen Y. Soliton, breather and rogue wave solutions for solving the nonlinear Schrödinger equation using a deep learning method with physical constraints. *Chin. Phys. B* 2021.

- [53] Pu JC, Li J, Chen Y. Solving localized wave solutions of the derivative nonlinear Schrödinger equation using an improved PINN method. *Nonlinear Dynam* 2021;105:1723–39.
- [54] Wang L, Yan ZY. Data-driven rogue waves and parameter discovery in the defocusing nonlinear Schrödinger equation with a potential using the PINN deep learning. *Phys. Lett. A* 2021;127408.
- [55] Fang Y, Wu GZ, Wang YY, Dai CQ. Data-driven femtosecond optical soliton excitations and parameters discovery of the high-order NLSE using the PINN. *Nonlinear Dynam.* 2021;105:603–16.
- [56] Baydin AG, Pearlmutter BA, Radul AA, Siskind JM. Automatic differentiation in machine learning: A survey. *J. Mach. Learn. Res.* 2018;18:1–43.
- [57] Liu DC, Nocedal J. On the limited memory BFGS method for large scale optimization. *Math. Program.* 1989;45:503–28.
- [58] Liu W, Zhang YS, He JS. Rogue wave on a periodic background for Kaup–Newell equation. *Rom. Rep. Phys.* 2018;70:106.
- [59] Ding CC, Gao YT, Li LQ. Breathers and rogue waves on the periodic background for the Gerdjikov–Ivanov equation for the Alfvén waves in an astrophysical plasma. *Chaos Solitons Fractals* 2019;120:259–65.
- [60] Stein ML. Large sample properties of simulations using latin hypercube sampling. *Technometrics* 1987;29(2):143–51.